Direct measurement of protein dynamics inside cells using a rationally designed photoconvertible protein

Tomoki Matsuda[1], Atsushi Miyawaki[2] & Takeharu Nagai[1]

All biological reactions depend on the diffusion and re-localization of biomolecules. Our understanding of biological processes requires accurate measurement of biomolecule mobility in living cells. Currently, approaches for investigating the mobility of biomolecules are generally restricted to measuring either fast or slow diffusion kinetics. We describe the development and application of a photoconvertible fluorescent protein, Phamret, that can be highlighted by UV light stimulation inducing a change in fluorescence emission from cyan fluorescent protein (CFP) to photoactivated GFP (PA-GFP). Phamret can be monitored by single excitation-dual emission mode for visualization of molecular dynamics for a broad range of kinetics. We also devised a microscopy-based method to measure the diffusion coefficient from the fluorescence decay after photostimulation of Phamret, enabling analysis of diffusion kinetics ranging from less than 0.1 μm^2/s up to ~ 100 μm^2/s, and found significant changes in free protein movement during cell-cycle progression.

Application of GFP and related fluorescent proteins has revolutionized our ability to analyze a wide range of biological processes such as gene expression, protein localization and cell motility in living specimens. Advances in fluorescence microscopy techniques have also enabled higher-resolution imaging of the fluorescence signals from fluorescent protein fusion constructs, providing insights into the movement of biomolecules and their interactions with cellular components[1,2].

Among these methods, imaging fluorescence resonance energy transfer (FRET) between two fluorescent proteins provides spatiotemporal information of protein-protein interactions and protein conformational changes in living cells[3]. FRET is the radiation-less energy transfer from an excited donor to an acceptor fluorophore that occurs when both molecules are in close proximity within ~ 10 nm at an appropriate orientation of the dipole moment. This technology has been used to develop genetically encoded fluorescent indicators for various cellular events[3].

Several microscopy techniques, including fluorescence correlation spectroscopy (FCS) and fluorescence recovery after photobleachi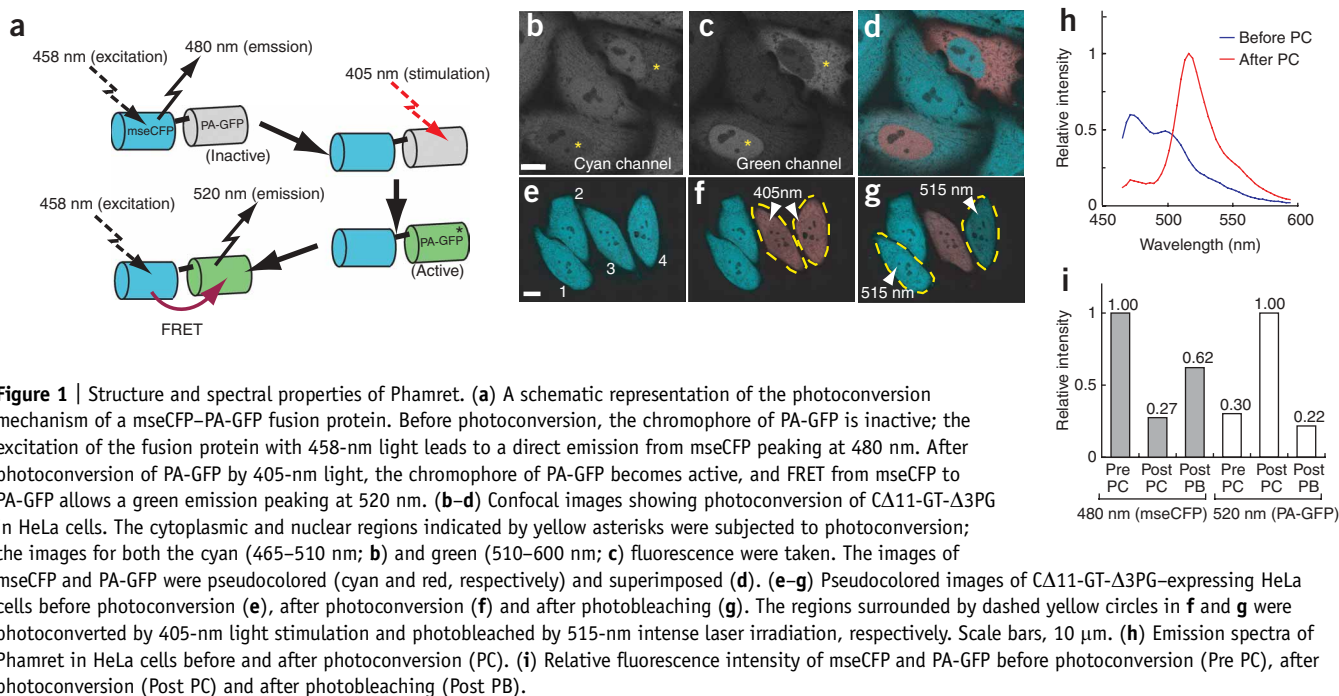ng (FRAP), are used to investigate mobility of biomolecules in living cells. FCS is used to determine the diffusion coefficient and the concentration of biomolecules in live cells by monitoring fluctuations in fluorescence intensity in a diffraction-limited spot of a laser beam[4]. FRAP is also used to investigate protein dynamics by photobleaching fluorescent molecules using a high-powered laser and then recording the movement of surrounding non-bleached fluorescent molecules into the photobleached area[5]. From the recovery curve, it is possible to estimate both the diffusion coefficient and immobile fraction of the tested proteins[6].

In recent years, various photosensitive fluorescent proteins have been developed by engineering existing fluorescent proteins or cloning new proteins from fluorescent organisms[7]. These photosensitive fluorescent proteins provide means to optically highlight selected proteins and to measure protein dynamics. Photosensitive fluorescent proteins can be classified into two types: photoactivatable and photoconvertible fluorescent proteins. Photoactivatable fluorescent proteins are those that are reversibly or irreversibly changed from a dark state to a bright state by photostimulation, such as PA-GFP[8], photoactivatable mRFP1 (ref. 9), KFP1 (ref. 10) and Dronpa[11]. In contrast, photoconvertible fluorescent proteins maintain a bright state but undergo an emission wavelength change from the pre- to post-photoconversion state by photostimulation. Examples of photoconvertible fluorescent proteins are Kaede[12], mEosFP[13], PS-CFP[14], KikGR[15] and Dendra[16]. The ability to detect both pre- and post-photoconversion states is a preferred characteristic for live-cell imaging, but all presently available photoconvertible fluorescent proteins undergo a change in excitation wavelength in addition to the shift in emission wavelength. This therefore requires a complicated microscope setup and also makes it difficult to measure rapid molecular dynamics. Furthermore, photoconvertible fluorescent proteins except PS-CFP, mEosFP and Dendra function as oligomers, which hinders their use as protein tags.

To overcome these problems, we rationally designed a monomeric photoconvertible fluorescent protein, Phamret, that requires only one wavelength to excite both the pre- and post-photoconverted states, thus enabling quantitative observation of rapidly diffusible molecules. We also developed a microscopy method, FDAP, for measurement of rapid diffusion of molecules, up to ~ 100 μm^2/s using Phamret or other photosensitive

Figure 1 | Structure and spectral properties of Phamret. (**a**) A schematic representation of the photoconversion mechanism of a mseCFP–PA-GFP fusion protein. Before photoconversion, the chromophore of PA-GFP is inactive; the excitation of the fusion protein with 458-nm light leads to a direct emission from mseCFP peaking at 480 nm. After photoconversion of PA-GFP by 405-nm light, the chromophore of PA-GFP becomes active, and FRET from mseCFP to PA-GFP allows a green emission peaking at 520 nm. (**b–d**) Confocal images showing photoconversion of CΔ11-GT-Δ3PG in HeLa cells. The cytoplasmic and nuclear regions indicated by yellow asterisks were subjected to photoconversion; the images for both the cyan (465–510 nm; **b**) and green (510–600 nm; **c**) fluorescence were taken. The images of mseCFP and PA-GFP were pseudocolored (cyan and red, respectively) and superimposed (**d**). (**e–g**) Pseudocolored images of CΔ11-GT-Δ3PG–expressing HeLa cells before photoconversion (**e**), after photoconversion (**f**) and after photobleaching (**g**). The regions surrounded by dashed yellow circles in **f** and **g** were photoconverted by 405-nm light stimulation and photobleached by 515-nm intense laser irradiation, respectively. Scale bars, 10 μm. (**h**) Emission spectra of Phamret in HeLa cells before and after photoconversion (PC). (**i**) Relative fluorescence intensity of mseCFP and PA-GFP before photoconversion (Pre PC), after photoconversion (Post PC) and after photobleaching (Post PB).

fluorescent proteins. The characteristic features of this method are (i) quick photostimulation time (0.25 ms); (ii) small light energy necessary for photostimulation (< 1 W/cm^2 in case of Phamret); (iii) fast acquisition of fluorescence decay (4,100 Hz) by reciprocal line scanning; and (iv) consideration of photobleaching during fluorescence decay measurement.

RESULTS

Design and evaluation of Phamret

To develop a photoconvertible fluorescent protein that can be excited by the same wavelength in both pre- and post-photoconversion states, we designed a fusion protein composed of a CFP variant (mseCFP) fused to a PA-GFP[8] (**Fig. 1a**). We designed this fusion protein to emit cyan fluorescence (480 nm) in the pre-photoconverted state, which can be shifted to green fluorescence (520 nm) by UV light stimulation of PA-GFP into a FRET acceptor for the mseCFP donor (**Fig. 1a**). This approach requires a high FRET efficiency between mseCFP and activated PA-GFP; otherwise no or small changes in fluorescence emission can be observed after UV stimulation. To achieve a high FRET efficiency, we concatenated mseCFP containing a C-terminal 11-amino-acid truncation to PA-GFP with a 3-amino-acid truncation from the N terminus via a dipeptide (Gly-Thr) linker. The bacterially expressed chimeric protein (CΔ11-GT-Δ3PG) exhibited a fivefold increase in the emission ratio (520 nm/480 nm) upon brief photoactivation by 420-nm pulsed laser. When expressed in living mammalian cells, CΔ11-GT-Δ3PG was distributed uniformly in both the cytoplasm and the nuclei (**Fig. 1b–d**). Spectral imaging revealed that all fluorescent cells had an emission spectrum identical to that of mseCFP, whereas upon 405-nm laser stimulation, the fluorescence emission in the stimulated area quickly changed from cyan to green, indicative of complete maturation of both mseCFP and PA-GFP in CΔ11-GT-Δ3PG at 37 °C (**Fig. 1e–g** and **Supplementary Fig. 1a–f** online). Upon activation, green fluorescence increased

3.3-fold, and cyan fluorescence emission decreased 3.7-fold, resulting in an approximately 12.2-fold ratio change between the pre- and post-photoconverted states (**Fig. 1h,i**). To confirm that the photoconversion of CΔ11-GT-Δ3PG was indeed due to FRET from mseCFP to activated PA-GFP, we bleached the acceptor PA-GFP. The decrease in PA-GFP emission peak was accompanied by dequenching of the mseCFP signal (**Fig. 1g–i** and **Supplementary Fig. 1g–i**), demonstrating that the dominant mechanism of the fluorescence color change in CΔ11-GT-Δ3PG was caused by FRET between mseCFP and activated PA-GFP. Therefore, we named this fusion protein Phamret for photoactivation-mediated resonance energy transfer. The photoconversion of Phamret was achieved using a lower laser power density (< 1 W/cm^2) than that for photobleaching. Accordingly, the quantum yield for photoconversion of Phamret was 2.7×10^{-2}, which was five times greater than that for the efficient highlighter, KikGR[15] (4.7×10^{-3}). pH titration of Phamret revealed that a high dynamic range (> 10-fold) was achieved in a neutral to alkaline environment ($> pH 7$), but it was strongly attenuated at acidic pH (**Supplementary Fig. 2a** online) and displayed a twofold dynamic range at pH 6.5. Phamret thus functions as a highlighter at physiological pH ranging from 6.5 to 8.0. Phamret was estimated to be a 53.4-kDa protein and is monomeric in living cells without displaying any unexpected binding to protein or proteolytic digestion (**Supplementary Fig. 2b–d**). Concordantly, Phamret in fusion with human β-actin and fibrillarin as well as targeting sequences for the Golgi bodies and the peroxisome showed an expected localization pattern (**Fig. 2a–d**) as reported previously[17–20]. In addition, the fusion proteins did not substantially perturb cellular functions such as cell division. Furthermore, all the fusion proteins tested underwent pronounced photoconversion by 405-nm laser illumination (**Fig. 2a–d**). Although we successfully labeled most of the proteins tested with Phamret, labeling of α-tubulin was unsuccessful (data not shown). Optimization of the amino-acid linker sequence and length between Phamret

and the protein of interest may resolve this problem. The properties of Phamret in comparison with other photoconvertible fluorescent proteins developed so far are shown in **Table 1**.

Cellular application of Phamret

To demonstrate the applicability of Phamret to stably label the intracellular structures, we expressed Phamret in mitochondria and took time-lapse images after Phamret photoconversion in one region. During a 15-min recording, a long thread-like mitochondrion fused and divided frequently, dramatically changing the pattern of the mitochondria network (**Fig. 2e–h** and **Supplementary Video 1** online). In parallel with the changes in the mitochondria structure, the shifted fluorescence color in the photoconverted region spread out and entered a surrounding mitochondrion. In addition, the labeled region in the fused mitochondrion was exchanged until it came to equilibrium at the intermediate color, indicating conjugation of the mitochondrial matrix and diffusion of the material in the fused mitochondrion.

We also observed positioning of chromosomes during mitosis in living mammalian cells. We labeled chromosomes in HeLa cells by expressing a histone 2B–Phamret fusion protein (H2B-Phamret). Owing to the very low dissociation rate of H2B from chromatin[21], the photoconverted marking remained detectable for many hours, allowing imaging of the dynamics of labeled chromosomes[22]. Just before mitosis, we photoconverted the nuclear halves and performed time-lapse imaging. In most cells (82%, $n = 14$), the global pattern of the mother cells was transmitted to the two daughter nuclei in G1 phase in a mirror-symmetric fashion (**Fig. 2i,j** and **Supplementary Video 2** online), indicating the heritability of chromosomal positions during cell division as previously shown by FRAP analysis using fluorescent protein tags in normal rat kidney cells[22].

Visualization of rapid protein dynamics using Phamret

All photoconvertible fluorescent proteins described to date undergo a change in excitation wavelength in addition to the shift in
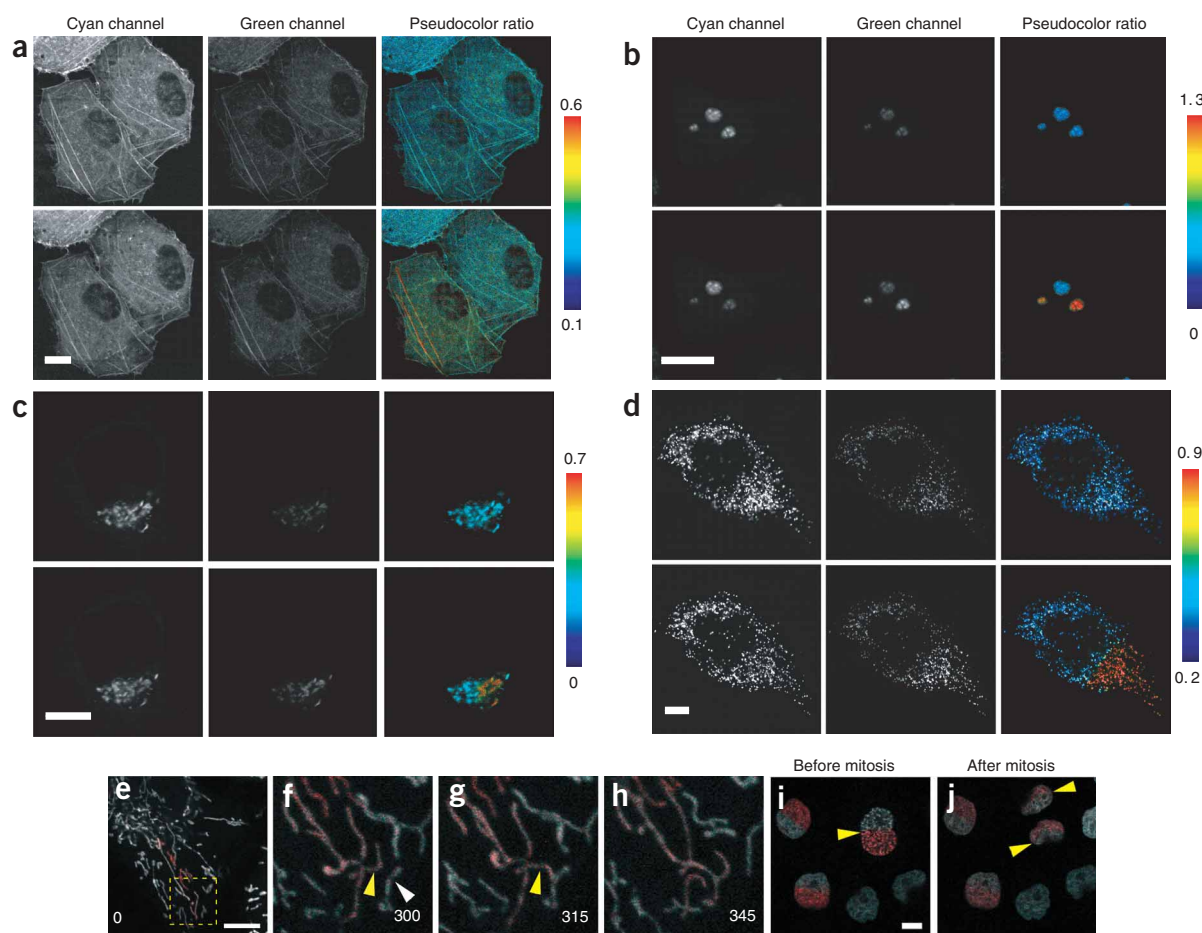
Figure 2 | Photoconversion of Phamret fusion protein in living cells. (**a–d**) Confocal fluorescence images of HeLa cells expressing Phamret fused to actin (**a**), fibrillarin (**b**), Golgi body localizing signal (**c**) and SKL tripeptide for peroxisome localization (**d**) before photoconversion (top) and after photoconversion (bottom) in the selected area, as shown in red (bottom right). The cyan channel, green channel and pseudocolored emission ratio (green to cyan) images are shown. Color bars represent green-to-cyan intensity ratio. (**e–h**) To track mitochondria, Phamret-expressing mitochondria in the selected area (as shown in red in **e**) were subjected to photoconversion (**e**). A yellow dashed box in **e** shows the region used for time-lapse imaging. Representative images taken at 300 s (**f**), 315 s (**g**) and 345 s (**h**) after photoconversion are shown. The yellow and white arrowheads in **f** indicate two mitochondria that were about to fuse. Arrowhead in **g** indicates the point of mitochondrial fusion, which was followed by spreading of Phamret protein in the fused mitochondrion (**h**). (**i,j**) Tracking of H2B-Phamret during mitosis. Half of the nucleus (arrowhead) being photoconverted just before mitosis (red; **i**). The daughter nuclei (arrowheads) show the preserved color pattern (**j**). Scale bars, 10 μm.

Table 1 | Properties of known photoconvertible proteins

Protein	Fluorescence color Before photoconversion / After photoconversion	Observed wavelength[a] (nm) Excitation	Emission	Stimulation Wavelength (nm)	Power density (W/cm²)	Fluorescence increase in ratio	Oligomeric status	Ref.
Phamret	Cyan	458	475	405	$<1^b$ ($\Phi_{PC} = 2.7 \times 10^{-2}$)[b]	$\sim 15^b$	Monomer	
	Green	458	517					
PS-CFP	Cyan	435	468	405	5–10	$\sim 1,500$	Monomer	14
	Green	490	511					
Kaede	Green	488	518	405	1.3	$\sim 2,000$	Tetramer	12
	Red	543	580					
KikGR	Green	488	517	405	~ 1 ($\Phi_{PC} = 4.7 \times 10^{-3}$)	NS	Tetramer	15
	Red	543	593					
EosFP	Green	488	516	405	NS	NS	Tetramer	13
	Red	543	581					
d2EosFP	Green	488	516	405	500	NS	Dimer	13
	Red	543	581					
mEosFP	Green	488	516	405	NS	NS	Monomer	13
	Red	543	581					
Dendra	Green	488	505	488	1.5	$\sim 1,500$–4,500	Monomer	16
	Red	543	575	405	0.6			
Cy11.5	Yellow	440	527	515 (bleaching)	$>10^b$	NS	Monomer	28
	Cyan	440	476					

Φ_{PC}, quantum yield for photoconversion. NS, not stated.
[a]Wavelength of excitation light for live imaging by microscopy and peak of emission spectrum. [b]Measured in our laboratory. A laser power meter was used to measure total power of the light after the objective lens. Light power density was estimated by dividing the total power by the area of the illuminated region.

emission wavelength upon photoconversion, and thus require measurement in dual excitation–dual emission mode. Generally, two different excitation wavelengths are alternated to obtain images both before and after photoconversion. This is unfavorable for observing rapidly diffusing molecules because of the acquisition time lag between two images. Even if we excite simultaneously the two states of photoconvertible fluorescent proteins, it is impractical because two lasers must be aligned to the same confocal spot by bringing two laser beams to a perfect and stable overlap. The single excitation property of Phamret overcomes this problem, but it may be possible to measure the presently available dual-excitation photoconvertible fluorescent proteins in single-excitation mode also. To address this, we compared the photoconversion contrast of Phamret with the dual-excitation photoconvertible fluorescent proteins, tandem dimer Dendra (td-Dendra), which is comparable in size to Phamret[16]. We expressed both proteins in HeLa cells, photoconverted them by 405-nm laser irradiation and simultaneously measured the change in fluorescence intensity of both pre- and post-photoconversion states at the frame rate of 41 Hz using an

appropriate excitation wavelength for each. At the first frame image after photoconversion, Phamret showed a 1.3-fold decrease and 2.4-fold increase in cyan and green fluorescence, respectively, yielding a 3.1-fold change in the emission ratio (**Supplementary Fig. 3a** online). The slower decrease in green fluorescence may be due to the photobleaching of PA-GFP moiety in Phamret. In contrast, td-Dendra had a 1.4-fold decrease in green fluorescence and no change in red fluorescence just after photoconversion, resulting in smaller contrast than for Phamret (**Supplementary Fig. 3b**). These results indicate that when using the single excitation–dual emission mode for fast frame acquisition, Phamret promises a higher contrast than Dendra. To further evaluate this,

Figure 3 | Visualization of rapid protein dynamics using Phamret. (**a**) Confocal images of donor CFP (top), acceptor PA-GFP (middle) and pseudocolored emission ratio (green/cyan; bottom) showing diffusion of photoconverted PP2Cγ-Phamret. Images were taken every 26 ms. (**b**) A magnified view of the first image just after photoconversion. The white circles (diameter 1.10 μm) represent ROIs used for intensity calculation. ROI 1 was set on the photoconverted circular region (diameter 1.38 μm). ROI 2 was placed outside of the photoconverted region. Distance between the centers of two ROIs is 2.1 μm. (**c**) Time course of cyan (solid line) and green (dashed line) fluorescence intensity of Phamret in ROI 1 (red) and ROI 2 (blue). (**d**) Time course of green to cyan emission ratio in ROI 1 and ROI 2. Scale bars, 10 μm.
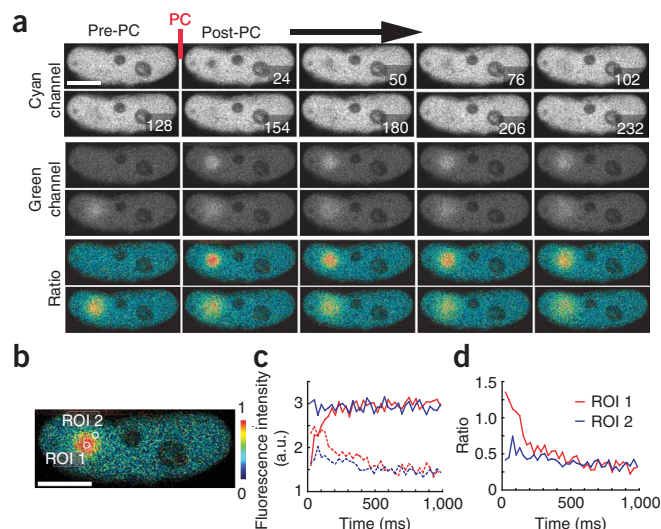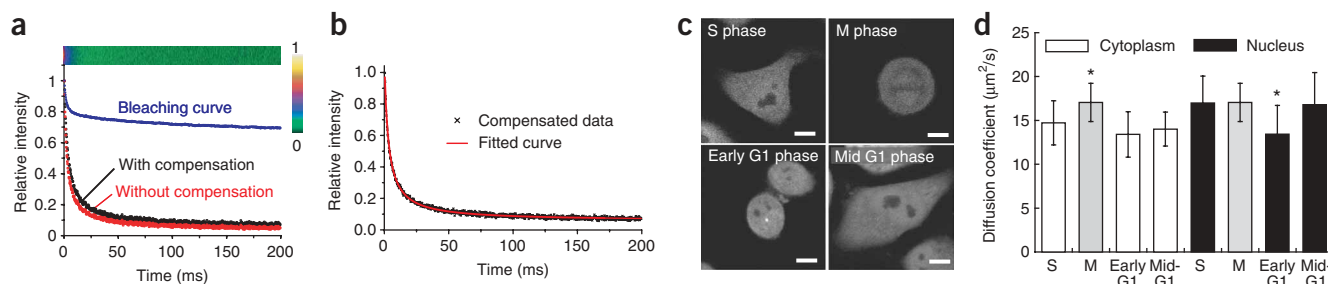
Figure 4 | Determination of diffusion coefficient of Phamret by FDAP. (**a**) Line-scanned images of photoconverted Phamret in solution were taken, and the kymographs of the images are shown in pseudocolor (top). Color bar indicates normalized fluorescence intensity. Average fluorescence decay curves in the solution were calculated (bottom). The blue curve represents the bleaching of photoconverted Phamret during image acquisition. (**b**) The compensated fluorescence decay curve determined by equation (3). (**c**) Fluorescence images of a cell at the indicated cell-cycle stages used for FDAP measurements. Scale bar, 10 μm. (**d**) Diffusion coefficient of Phamret in the cytoplasm and the nucleus at the indicated cell-cycle stages. In the case of M phase, the same data are shown (light gray bars) because the cytoplasm and nucleus cannot be distinguished due to the disappearance of the nuclear membrane. Asterisks (*) indicate the cell phase where the diffusion coefficient is significantly different from other phases in either the cytoplasm or nucleus, respectively. Error bars are s.d. ($n > 10$). Validity of the differences was statistically confirmed by one-way analysis of variance (ANOVA) and defined as significant at $P = 4.0 \times 10^{-6}$ and 4.1×10^{-4}, respectively. Differences between cytoplasm and nucleus in S and G1 phase were also confirmed by using two-sided t-test ($P = 0.005$ and 0.008) with significance level $\alpha = 0.05$.

we examined a PP2Cγ-Phamret fusion protein in the nucleus of a HeLa cell. After photoconversion of PP2Cγ-Phamret in a region of the nucleus, we acquired fluorescence images at 41 Hz that show how fast the photoconverted PP2Cγ-Phamret diffuses (**Fig. 3** and **Supplementary Video 3** online).

Determination of biomolecule diffusion coefficients

To determine diffusion coefficients of proteins tagged with photo-sensitive fluorescent proteins, we devised a new microscopy technique that enables measurement of a wide range of diffusion coefficients. This technique, FDAP, is based on measurement of fluorescence decay after photostimulation of photosensitive fluor-escent proteins by quick (0.25 ms) photo-irradiation using a focused laser followed by repeated reciprocal line scanning at 4,100 Hz. We used a laser confocal microscope equipped with a dual laser scanner to carry out photostimulation during fluores-cence measurement. We used Phamret as the photosensitive fluorescent protein, and measured the diffusion coefficient in aqueous solution (**Fig. 4a**). When we used averaged fluorescence decay data derived from 10 measurements directly for fitting by Eq. 3, the estimated diffusion coefficient was 70.4 ± 0.8 μm²/s. This value is much larger than 50.4 μm²/s determined by FCS for the GFP tandem dimer[23]. Because the FDAP experiment required about ten times more intense laser irradiation for excitation than that used in FRAP to acquire line images with a high-enough signal-to-noise ratio, we speculated that the difference in measured diffusion coefficients was due to photobleaching of PA-GFP moiety in Phamret during the fluorescence decay measurement (**Supplementary Fig. 3a**). To estimate the influence from photobleaching, we recorded a time course of fluorescence intensity using fully photoconverted Phamret in solution or in a cell in which we

neglected the fluorescence decay caused by the molecular diffusion. Although the fluorescence attenuation rate in FDAP was larger than that expected from simple bleaching immediately after starting the measurement, the total number of bleached molecules was comparable between FDAP and FRAP at the end of measurements (**Supplementary Fig. 4a,b** online). We used the measured decay curve (**Fig. 4a**) for data compensation and applied the compensated data for nonlinear curve fitting (**Fig. 4b**). The diffusion coefficient after correction was 49.5 ± 0.6 μm²/s, which was almost equivalent to the previous FCS data[23]. Recently, a method to measure faster diffusion using FRAP by attempting to account for the finite time of the photobleaching has been proposed[24]. Therefore, we performed FRAP measurements to compare the results with those of FDAP (**Supplementary Fig. 4c–f**) and FCS analyses. All three methods gave comparable results for tandem fluorescent protein dimers (**Table 2**). However, the diffusion coefficient of a single fluorescent protein measured by FRAP was substantially different from those obtained by FDAP and FCS, indicating that FDAP may be more reliable than FRAP for analysis of fast-diffusing molecules with >20 μm²/s diffusion coefficient, provided that an accurate bleaching curve can be obtained for correction of the FDAP data (**Table 2**).

To validate the performance of FDAP, we compared the diffusion coefficient of Phamret in HeLa cells at different stages of the cell cycle (S/G2, M, early G1 and mid-G1) as well as in different compartments, cytoplasm and nucleus (**Fig. 4c**). We obtained a correction curve for this experiment using fully photoconverted Phamret in HeLa cells. Generally, the diffusion coefficient of Phamret in the nucleus was greater than that in cytoplasm except in early-G1 phase in which Phamret in both nucleus and cytoplasm showed a similar diffusion coefficient (**Fig. 4d**). Furthermore, we found that the diffusion coefficients in the nucleus during early-G1 phase (13.4 ± 3.3 μm²/s) were significantly smaller than those in other phases (17.0 ± 3.1 in S phase, 17.1 ± 2.2 in M phase, 16.8 ± 3.7 in mid-G1 phase; **Fig. 4d**). Although the cells in M phase are classified into neither cytoplasm nor nucleus because both com-partments are mixed after disappearance of the nuclear membrane, the diffusion coefficient of Phamret in M phase tends to show the

Table 2 | Comparison of FDAP with other methods

Fluorescent protein	FDAP D (μm²/s)	FRAP D (μm²/s)	FCS D (μm²/s)
Single	22.9 ± 3.7	34.0 ± 8.5	23.4 ± 2.5
Tandem dimer	14.1 ± 2.4	18.3 ± 6.4	16.4 ± 0.8

value for S and mid-G1 phase nucleus, suggesting that the cellular environment of the M-phase cell was more nuclear-like than cytoplasm-like.

DISCUSSION

The microscopy method we developed, FDAP, allowed reliable measurement of diffusion coefficients up to $\sim100\ \mu m^2/s$, the measurement of which has been quite difficult using FRAP. The reason why FRAP gave a different diffusion coefficient in the comparison of FDAP and FCS, may be due to the use of the first frame image after photobleaching to calculate the bleaching constant in FRAP[24]. The first frame image after photobleaching contains irrelevant diffusion data obtained during the photobleaching and the first image acquisition. Thus, this may affect the calculation of the bleaching constant, especially for fast-diffusing molecules, resulting in an overestimation of the diffusion coefficient. According to reference 25, the total bleaching time should be at least 15 times smaller than the characteristic recovery time[25]. The photostimulation time of 0.25 ms in our FDAP measurement is brief enough that the diffusion during photostimulation can be neglected. Moreover, the FRAP measurement has other drawbacks: the bleaching constant needs to be determined whenever the target molecules or intracellular environment are changed because the value of the bleaching constant depends on the diffusion constant of the target molecules. In the presence of a highly immobile fraction, the bleaching profile in the first image contains contributions of both the diffusing mobile fraction and the stationary immobile fraction, requiring complex assumptions[24]. Our FDAP method is not affected by this issue.

Compared to FCS, FDAP has the advantage of retrieving additional information regarding the states of the immobile molecules. FDAP can be used to investigate any diffusion kinetics ranging from $<0.1\ \mu m^2/s$ to $\sim100\ \mu m^2/s$. Notably, when compared with FCS, measurement time for a fast diffusible protein ($>10\ \mu m^2/s$) by FDAP is much shorter (200 ms for FDAP versus >10 s FCS[23]), which is an advantage when analyzing molecules that quickly change diffusion coefficient upon stimulation.

In the post genomic era, many cascade maps for signal transduction pathways activated by biological events have been described. These maps are very useful for understanding the mechanisms of cellular activity at the molecular level. Information on protein and molecule movement rates within cells provides enhanced understanding of not only signal transduction but also various physiological phenomena at the molecular level. The ability to measure molecular mobility over a broad kinetic range with this single technique provides a useful complement to FRAP or FCS, thus benefiting studies on molecular dynamics in living cells.

METHODS

Imaging. For cell imaging we used an Olympus confocal inverted microscope FV1000 equipped with UPLSAPO $60\times$ 1.35 numerical aperture (NA) oil objective and multi-Argon ion laser. We used a 405 nm laser diode for photostimulation. We acquired the cyan and green fluorescence signals by excitation at 458 nm and detected them at 465–510 nm and 510–600 nm wavelength range, respectively. For td-Dendra imaging, we simultaneously acquired the green (495–525 nm) and red fluorescence (560–650 nm) signals by excitation at 488 nm. We created the fluorescence ratio images using AquaCosmos software (Hamamatsu Photonics).

Determination of diffusion coefficient by FDAP. We estimated the activation characteristics of the laser using fixed cells expressing Phamret. First, we photoconverted Phamret in a fixed cell by the pulse irradiation with a 405-nm laser for 0.25 ms, and measured fluorescence intensity. Then we photoconverted the whole region of the same cell again until the fluorescence came to equilibrium, and again measured the fluorescence intensity. We divided the fluorescence intensity of once-photoconverted Phamret at the position (r) from the center of the activated region by the fluorescence intensity of fully photoconverted Phamret. We fitted the divided values at different positions to the Gaussian laser profile modified from the previously published one[26] so that the center of the activation profile became the peak value of fluorescence intensity as described by following equation:

$$C(r) = 1 - \exp\left(-K \exp\left(-\frac{2r^2}{w^2}\right)\right), \qquad (1)$$

where $C(r)$ is the concentration of the photoconverted Phamret, K is the activation constant for the fixed cells, and w is the half-width of the laser beam at $1/e^2$ intensity.

Each FDAP experiment started with image scans, followed by a 405-nm laser irradiation for 0.25 ms on a point in the scanning area. We collected a series of line scanned images of the fluorescence emission in the region of 510–600 nm at 0.244 ms intervals ($\approx4{,}100$ Hz) for 200 ms using 488-nm laser as excitation light. We skipped the first line scanning image to avoid direct influence of the irradiated pulse of the 405 nm laser. We fixed the length of line scanning to 80 pixels, and each pixel width was 103 nm. We used the central 8 pixels (0.824 μm) in the scanned line as a region of interest for the fluorescence intensity measurement. We calculated the background signals as the average intensity in the region of interest, which we measured 50 ms before photoconversion. We calculated the average fluorescence in the region of interest (ROI) at time t after the photoconversion, $I_{\text{ROI}}(t)$, from each line image with the subtracted background signal. The fluorescence signal measured in a region of interest normalized to the change in total fluorescence was determined as

$$I_{\text{rel. image}}(t) = \frac{I_{\text{ROI}}(t)}{I_{\max}}, \qquad (2)$$

where $I_{\max}$ is the maximum intensity after the photoconversion.

Because the measured fluorescence decay contains contribution from photobleaching, the original fluorescence decay data must be compensated. To do this, we measured a time course of the photobleaching of completely photoconverted Phamret. We then divided the originally acquired decay curve by the photobleaching curve and used the recalculated data for the curve fitting. Using the values of K and w, we fitted the FDAP decay curves of $I_{\text{rel. image}^*}(t)$ to the decay function, $I_{\text{rel. calc.}}(t)$ modified from that reported for FRAP[27]:

$$I_{\text{rel. image}^*}(t) = \alpha \times I_{\text{rel. calc}}(t)$$
$$= \alpha\left(1 - \left((1-\beta)\sum_{n=0}^{+\infty}\frac{(-K)^n}{n!}\left(1 + n\left(1 + \frac{2t}{\tau_D}\right)\right)^{-1} + \beta\frac{1 - e^{-K}}{K}\right)\right) \qquad (3)$$

where α is a parameter to conform $I_{\text{rel. calc.}}$ to $I_{\text{rel. image}^*}$ at $t = 0$ and β is the fraction of immobile molecules (ranging from 0 to 1).

τ_D is the characteristic diffusion time related to the diffusion coefficient, D, by $\tau_D = w^2/4D$. The series solution for the fluorescence decay was truncated after 40 terms[18], assuring that the neglected terms made an insignificant contribution. All of the curve fittings were done by using a weighted least-squares algorithm implemented in Origin (OriginLab).

Additional methods. The methods for plasmid construction, cell culture and transfections, protein purification, gel filtration, spectroscopy, pH titration, measurement of photoconversion quantum yield and western blotting are available in **Supplementary Methods** online.

Note: Supplementary information is available on the Nature Methods website.

AUTHOR CONTRIBUTIONS
T.M. performed experiments, analyzed data and prepared the manuscript; A.M. contributed to data analysis; T.N. contributed to the conceptual development and experimental design and performed experiments, analyzed data and prepared the manuscript.

Published online at http://www.nature.com/naturemethods/
Reprints and permissions information is available online at
http://npg.nature.com/reprintsandpermissions

1. Lippincott-Schwartz, J., Snapp, E. & Kenworthy, A. Studying protein dynamics in living cells. *Nat. Rev. Mol. Cell Biol.* **2**, 444–456 (2001).
2. Zhang, J., Campbell, R.E., Ting, A.Y. & Tsien, R.Y. Creating new fluorescent probes for cell biology. *Nat. Rev. Mol. Cell Biol.* **3**, 906–918 (2002).
3. Miyawaki, A. Visualization of the spatial and temporal dynamics of intracellular signaling. *Dev. Cell* **4**, 295–305 (2003).
4. Medina, M.A. & Schwille, P. Fluorescence correlation spectroscopy for the detection and study of single molecules in biology. *Bioessays* **24**, 758–764 (2002).
5. Reits, E.A. & Neefjes, J.J. From fixed to FRAP: measuring protein mobility and activity in living cells. *Nat. Cell Biol.* **3**, E145–E147 (2001).
6. White, J. & Stelzer, E. Photobleaching GFP reveals protein dynamics inside live cells. *Trends Cell Biol.* **9**, 61–65 (1999).
7. Lukyanov, K.A., Chudakov, D.M., Lukyanov, S. & Verkhusha, V.V. Innovation: Photoactivatable fluorescent proteins. *Nat. Rev. Mol. Cell Biol.* **6**, 885–891 (2005).
8. Patterson, G.H. & Lippincott-Schwartz, J. A photoactivatable GFP for selective photolabeling of proteins and cells. *Science* **297**, 1873–1877 (2002).
9. Verkhusha, V.V. & Sorkin, A. Conversion of the monomeric red fluorescent protein into a photoactivatable probe. *Chem. Biol.* **12**, 279–285 (2005).
10. Chudakov, D.M. *et al.* Kindling fluorescent proteins for precise *in vivo* photolabeling. *Nat. Biotechnol.* **21**, 191–194 (2003).
11. Ando, R., Mizuno, H. & Miyawaki, A. Regulated fast nucleocytoplasmic shuttling observed by reversible protein highlighting. *Science* **306**, 1370–1373 (2004).
12. Ando, R., Hama, H., Yamamoto-Hino, M., Mizuno, H. & Miyawaki, A. An optical marker based on the UV-induced green-to-red photoconversion of a fluorescent protein. *Proc. Natl. Acad. Sci. USA* **99**, 12651–12656 (2002).
13. Wiedenmann, J. *et al.* EosFP, a fluorescent marker protein with UV-inducible green-to-red fluorescence conversion. *Proc. Natl. Acad. Sci. USA* **101**, 15905–15910 (2004).
14. Chudakov, D.M. *et al.* Photoswitchable cyan fluorescent protein for protein tracking. *Nat. Biotechnol.* **22**, 1435–1439 (2004).
15. Tsutsui, H., Karasawa, S., Shimizu, H., Nukina, N. & Miyawaki, A. Semi-rational engineering of a coral fluorescent protein into an efficient highlighter. *EMBO Rep.* **6**, 233–238 (2005).
16. Gurskaya, N.G. *et al.* Engineering of a monomeric green-to-red photoactivatable fluorescent protein induced by blue light. *Nat. Biotechnol.* **24**, 461–465 (2006).
17. Ballestrem, C., Wehrle-Haller, B. & Imhof, B.A. Actin dynamics in living mammalian cells. *J. Cell Sci.* **111**, 1649–1658 (1998).
18. Phair, R.D. & Misteli, T. High mobility of proteins in the mammalian cell nucleus. *Nature* **404**, 604–609 (2000).
19. Llopis, J., McCaffery, J.M., Miyawaki, A., Farquhar, M.G. & Tsien, R.Y. Measurement of cytosolic, mitochondrial, and Golgi pH in single living cells with green fluorescent proteins. *Proc. Natl. Acad. Sci. USA* **95**, 6803–6808 (1998).
20. Recalcati, S., Menotti, E. & Kühn, L.C. Peroxisomal targeting of mammalian hydroxyacid oxidase 1 requires the C-terminal tripeptide SKI. *J. Cell Sci.* **114**, 1625–1629 (2001).
21. Kimura, H. & Cook, P.R. Kinetics of core histones in living human cells: little exchange of H3 and H4 and some rapid exchange of H2B. *J. Cell Biol.* **153**, 1341–1353 (2001).
22. Gerlich, D. *et al.* Global chromosome positions are transmitted through mitosis in mammalian cells. *Cell* **112**, 751–764 (2003).
23. Pack, C., Saito, K., Tamura, M. & Kinjo, M. Microenvironment and effect of energy depletion in the nucleus analyzed by mobility of multiple oligomeric EGFPs. *Biophys. J.* **91**, 3921–3936 (2006).
24. Braga, J., Desterro, J.M.P. & Carmo-Fonseca, M. Intracellular macromolecular mobility measured by fluorescence recovery after photobleaching with confocal laser scanning microscopes. *Mol. Biol. Cell* **15**, 4749–4760 (2004).
25. Meyvis, T.K., De Smedt, S.C., Van Oostveldt, P. & Demeester, J. Fluorescence recovery after photobleaching: a versatile tool for mobility and interaction measurements in pharmaceutical research. *Pharm. Res.* **16**, 1153–1162 (1999).
26. Axelrod, D., Koppel, D.E., Schlessinger, J., Elson, E. & Webb, W.W. Mobility measurement by analysis of fluorescence photobleaching recovery kinetics. *Biophys. J.* **16**, 1055–1069 (1976).
27. Calapez, A. *et al.* The intranuclear mobility of messenger RNA binding proteins is ATP dependent and temperature sensitive. *J. Cell Biol.* **59**, 795–805 (2002).
28. Shimozono, S. *et al.* Concatenation of cyan and yellow fluorescent proteins for efficient resonance energy transfer. *Biochemistry* **45**, 6267–6271 (2006).